Metals and Materials International (2021) 27:2095–2105
https://doi.org/10.1007/s12540-020-00733-6

Study on Formation of Microstructure in Rheo-Diecastings of Semi-Solid A380 Aluminum Alloy Slurry

Zhiyong Liu[1,2] · Guotao Cui[1] · Tan Wan[3] · Weimin Mao[2]

Received: 10 March 2020 / Accepted: 14 April 2020 / Published online: 19 May 2020
© The Korean Institute of Metals and Materials 2020

Abstract
The formation of the microstructure in the rheo-diecastings were studied by the experiment of rheo-diecasting with semi-solid A380 Aluminum alloy slurry. The results show that the grain diameter and shape factor of primary α-Al grains decreased and increased along the rheo-diecasting direction, respectively, making the primary α-Al grains gradually distributing uniformly. The combination of injection pressure and narrow gate of the runner and ingate was the main reason for the evolution of the primary α-Al grains, moreover, the collision and friction among primary α-Al grains during the filling were helpful for the refinement and spheroidization of the primary α-Al grains. The residual liquid solidified into the secondary solidification microstructure accompanied by the evolution of the primary α-Al grains. The accumulation of the fragments of the primary α-Al grains, the secondary α_2-Al nuclei or grains which formed in previous positions, the effective nucleation rate of the residual liquid, and the collision and fraction among the secondary α_2-Al grains and between the secondary α_2-Al grain and the primary α-Al grains made the secondary solidification microstructure of the residual liquid present multiplex and complicate characteristics.

Keywords Semi-solid slurry · A380 aluminum alloy · Rheo-diecasting · Evolution of primary α-al grains · Secondary solidification of residual liquid

1 Introduction

The semi-solid slurry possesses the high viscosity and low superheating [1], which makes semi-solid slurry fill the mold cavity in laminar flow, resulting in the oxidation inclusion, shrinkage porosity and macro segregation being reduced effectively in rheo-diecastings [2–4]. Moreover, the rheo-diecastings with the smaller shrinkage, higher density and lower cost compares with the vacuum die casting [5, 6] and pore-free die casting [7, 8], so it has a broad application prospect. At present, most researches on the rheo-diecasting mainly focus on the process parameters of the rheo-diecasting [9], filling capacity [10, 11] and mechanical properties [12, 13], but lacks those on the formation of the microstructure. General speaking, the liquid fraction of semi-solid slurry during filling is greater than 50% [14, 15], which means that the formation of the microstructure in rheo-diecastings involves the evolution of primary α-Al grains and the secondary solidification of residual liquid. Without doubt that when the semi-solid slurry passed through the narrow gate, the primary grains are broken and fractured easily, furthermore, the friction and collision among the primary and secondary grains also affect the refinement and spheroidization of the primary grains [16, 17]. However, the essential factors and mechanism that affects the evolution of primary grains need to be studied deeply. The solidification of the residual liquid in semi-solid slurry during rheo-diecasting was very different from that of the melt during traditional die casting [18, 19]. Moreover, there are different views on the secondary solidification of the residual liquid. Fan [20, 21] pointed out that the shearing in the preparation of the semi-solid slurry can affect the secondary solidification of the residual liquid, meanwhile, he stressed that the secondary nucleation was independent and the secondary nucleus growing in a steady before the completion of the secondary solidification, which made the secondary grains be the near-spherical.

✉ Zhiyong Liu
yyaffe@126.com

[1] School of Mechanical and Electrical Engineering, Heze University, Heze 274015, Shandong, China

[2] School of Materials Science and Engineering, University of Science and Technology Beijing, Beijing 100083, China

[3] School of Materials Science and Engineering Beijing, University of Tsinghua, Beijing 100084, China

But Li [22, 23] held that the preparation parameter of semi-solid slurry has no influence on the secondary solidification of the residual liquid, and there are three ways for the growth of the secondary nucleus, i.e. the steady, unsteady and merge growth. However, above mentioned viewpoints based on the different preparation processes of the semi-solid slurry. Therefore, the solidification of residual liquid and the evolution of the secondary grains needs more extensive study.

In this paper, semi-solid A380 Aluminum alloy slurry was prepared by a graphite serpentine channel [24], and the rheo-diecastings of semi-solid A380 Aluminum alloy slurry was produced. The evolution distribution of the primary α-Al grains during rheo-diecasting were studied by analyzing the change of microstructure at the different positions of the rheo-diecastings along its rheo-diecasting direction. Meanwhile, the secondary solidification behavior of the residual liquid and the evolution of the secondary α_2-Al grains was studied by comparing the microstructures of the center region and edge region of the same cross section in the rheo-diecastings and comparing the microstructures of the different positions along the rheo-diecasting direction.

2 Experiments

2.1 Materials

Commercial A380(YL112) Aluminum Alloy was used as experimental material, whose chemical compositions were shown in Table 1. Its solid–liquid temperature rang was from 525 to 597 ℃, as shown in Fig. 1, which was test by a differential scanning calorimeter, and whose heating rate was10 ℃/min during the test.

2.2 Methods

Firstly, the A380 aluminum alloy was put in a graphite clay crucible and melted to a fixed temperature by a resistance furnace. When the melt was cooled to 630 ℃, it was poured into a serpentine channel that was assembled by two symmetrical graphite blocks which had five bends whose inner diameter was 25 mm. The melt in the serpentine channel became the semi-solid slurry under the chilling effect of the inner wall and the self-stirring of the melt. The temperature of the semi-solid slurry that flew out the serpentine channel was about 572 ℃ that was measured by the thermocouple, and the corresponding

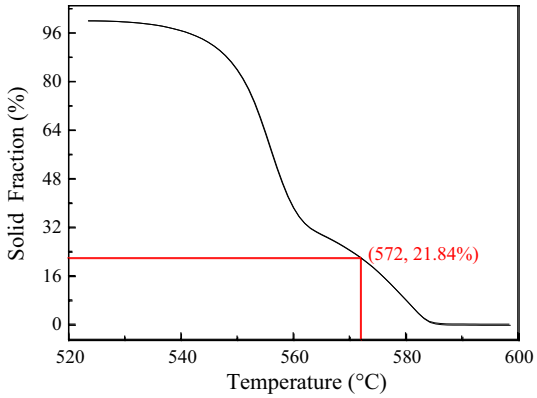

Fig. 1 Curve of solid fraction vs temperature

solid fraction was about 20%, as shown in Fig. 1. The semi-solid slurry was collected and transferred into the shot sleeve ($\Phi 57 \times l350$ mm) by a preheating heat-insulated ladle within 3 s. The semi-solid slurry was filled into the mold cavity from shot sleeve through the runner and ingate under the injection pressure, the injection pressure was 70 MPa without intensification of pressure, the slow and fast shot speeds of the plunger were 0.5 m/s and 2 m/s respectively, and the filling speed at the ingate was about 16 m/s. What's more, the diameter of the plunger was 55 mm and the section area of the ingate was 4×(18 mm×4 mm). The schematic of the semi-solid slurry preparation and rheo-diecasting was shown in Fig. 2. Before rheo-diecasting, the shot sleeve and mold were preheated to about 350 ℃ and 200 ℃, respectively.

And then, the specimens A, B, C, D, E and F were got at the different positions along the rheo-diecasting direction, as shown in Fig. 3. In order to study the evolution of the primary α-Al grains, the secondary solidification of the residual liquid and the evolution of the secondary α_2-Al grains, the edge regions and center regions of specimens A–F were fabricate into the standard metallographic specimens after polishing and etching. Finally, the microstructures of the above mentioned metallographic specimens were observed and analyzed by Neuphoto21 optical microscope and Image-Pro Plus analysis software, respectively. The grain diameter and shape factor of the primary α-Al grains were calculated by $D=(4A/\pi)^{1/2}$ and $F_s=4A/C^2$ respectively. Where D, F_s, A, N, and C are the grain diameter, shape factor, area and perimeter of the primary α-Al grain, respectively [24].

Table 1 Chemical compositions of A380 aluminum alloy (wt%)

Si	Cu	Fe	Mn	Mg	Zn	Others	Al
7.83	3.2	0.21	0.46	< 0.1	< 0.07	< 1.0	Bal

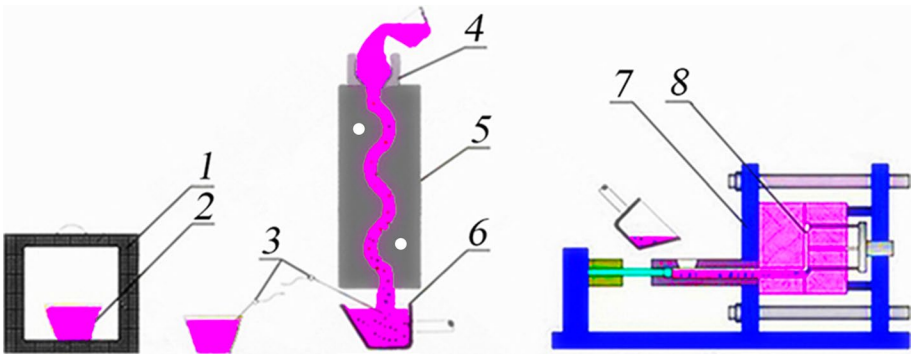

Fig. 2 Schematic diagram of the semi-solid slurry preparation and rheo-diecasting. 1. Resistance furnace; 2. Graphite clay melting crucible; 3. Thermocouple; 4. Pouring cup; 5. Serpentine channel; 6. Heat preservation ladle; 7. Horizontal die casting machine; 8. Mold cavity

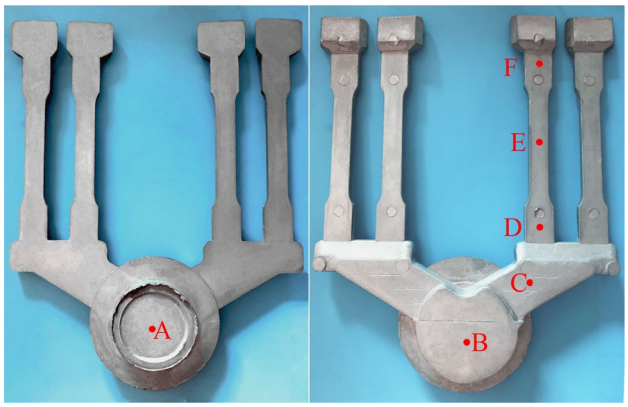

Fig. 3 Different positions along the rheo-diecasting direction

3 Results

3.1 Microstructure of the Biscuit

Figure 4a was the microstructures in center region of the biscuit front-end that was marked "A" in Fig. 3. The big white particles were primary α-Al grains, the dark region and small size particles among the primary α-Al grains were secondary solidification microstructure of the residual liquid. The primary α-Al grains accounted for most of the area in two dimension, moreover, the most of the primary α-Al grains were near-spherical and rose-like except a few of the degenerated dendrites or dendritic arms, as shown in Fig. 4a. The grain diameter and shape factor were 42 μm and 0.72 respectively. The residual liquid mainly solidified into the protrusions of the primary α-Al grains, which was quite different from those in the references [20–23]. They rapidly grew into the developed dendrites, the length of the principal axis reached 10 μm under free growth, as shown by arrow in Fig. 4a. However, in some regions, the protrusions grew and touched each other, which formed a region mixture with the granular and equiaxed grains, as shown by rectangle in Fig. 4a. The area proportion of the primary α-Al grains decreased in two dimension with the semi-solid slurry solidified into the back-end of the biscuit that was marked "B" in Fig. 3. The morphology of the primary α-Al grains changed slightly, and they tended to aggregate in certain direction, as shown in Fig. 4c. The primary α-Al grains mainly consisted of the near-spherical, rose-like grains besides a few of degenerated dendrites. The grain diameter and shape factor reduced to 41 μm and improved to 0.73 respectively. Compared with the front-end, the secondary α_2-Al grains had undergone a certain evolution, which made the secondary α_2-Al grains have the different morphology in local regions, as shown in Fig. 4c. There were three representative region in Fig. 4c, the region dominated by the fine developed dendrites was shown by arrow, the region of the mixture of the fine dendrites and protrusions was shown by rectangle, and the mixture region with protrusions, granular and equiaxed grains was shown by ellipse, which was mainly related to that the fragments of the primary α-Al grains and secondary α_2-Al grains were brought into the semi-solid slurry.

Both the primary α-Al grains and secondary α_2-Al grains in edge region were different from those in center region either in front-end or in back-end of the biscuit. In edge region of the biscuit front-end, the area proportion of the primary α-Al grains decreased obviously. Even so, there were a quite number of the primary α-Al grains distributed in the outmost edge region. The primary α-Al grains composed of the near-spherical, rose-like grains and a few of degenerated dendrites, whose shape factor and grain diameter improved and reduced to 0.74 and 40 μm, respectively. The residual liquid solidified into the fine equiaxed secondary α_2-Al grains and the short protrusions, as shown in Fig. 4b. With the filling of semi-solid slurry, the number of the primary α-Al grains decreased significantly in edge region of back-end, and the primary α-Al grains were rarely brought into the outmost edge region. With the degenerated dendrites disappeared completely, the primary α-Al grains were mainly near-spherical. The grain diameter and shape factor were 39 μm and 0.75 respectively. The morphology of the

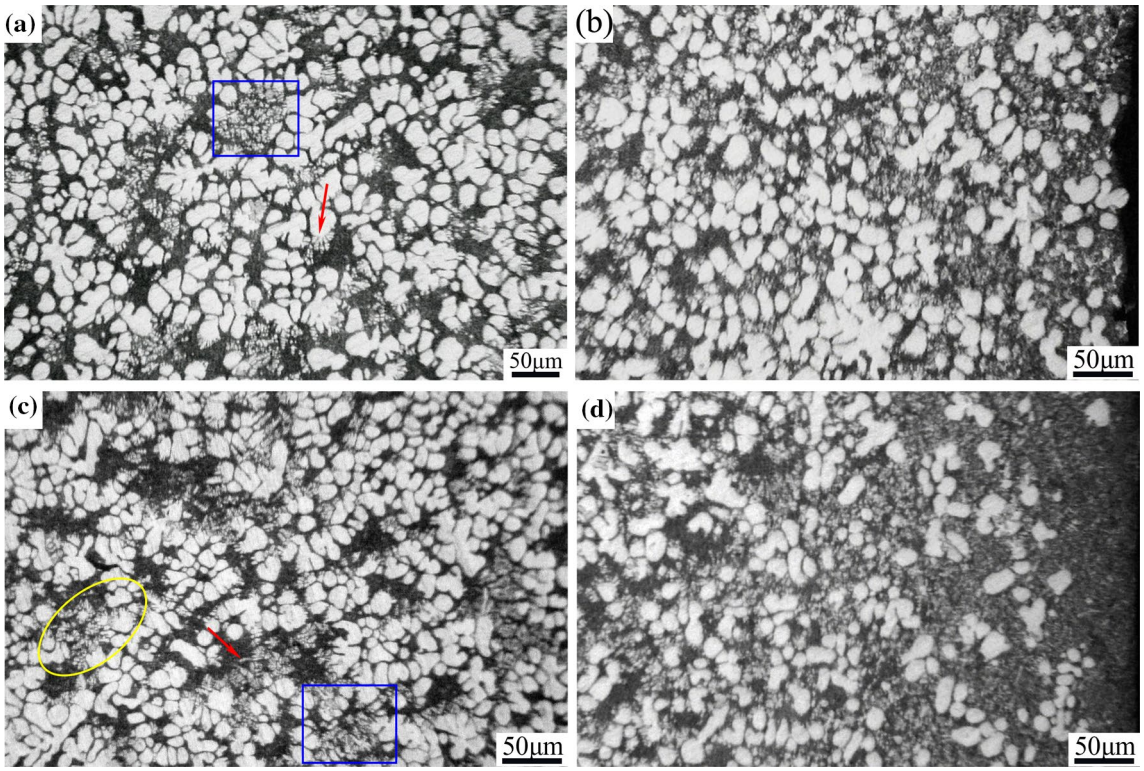

Fig. 4 Microstructures of the biscuit. **a** Center region of the biscuit front-end; **b** edge region of the biscuit front-end **c** center region of the biscuit back-end; **d** edge region of the biscuit back-end

secondary α_2-Al grains was diverse, which was composed of the super fine dendrites, granular and equiaxed grains.

3.2 Microstructure of the Runner

When the semi-solid slurry filled into the runner that was shown by "C" in Fig. 3, the area proportion of the primary α-Al grains in center region increased obviously because of the blocking of the narrow gate, as shown in Fig. 5a. At same time, the impact stress from injection pressure made the dendrites break or bend from the necking at the root of the dendritic arms [25], as shown by "1"–"4" in Fig. 5a. Moreover, the collision and friction among the primary α-Al grains made themselves get further spheroidization and refinement. As a result, the primary α-Al grains were mainly spherical, near-spherical and rose-like, whose grain diameter and shape factor were 39 μm and 0.75, respectively. With the primary α-Al grains increased, the secondary α_2-Al grains decreased significantly, and they mostly consisted of the granular secondary α_2-Al grains and short rod-like

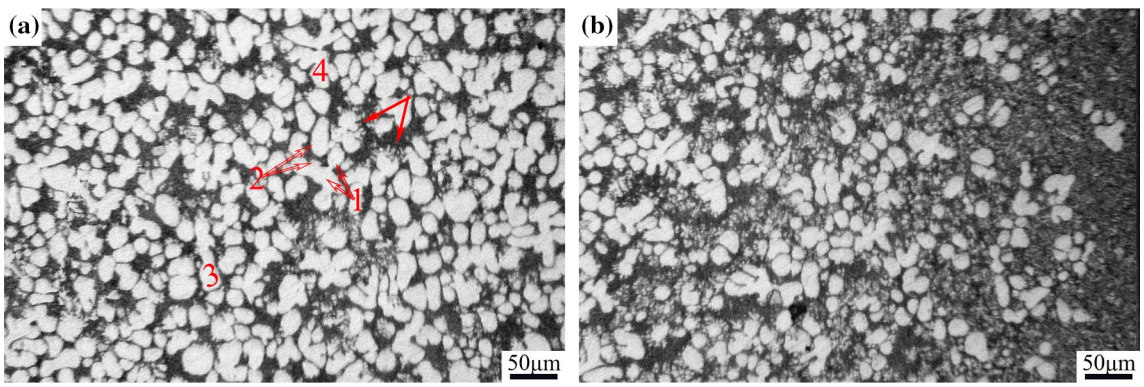

Fig. 5 Microstructures of the runner **a** center region of the runner; **b** edge region of the runner

protrusions, moreover, the short rod-like protrusions reformed only locally because of a few of the residual liquid, as shown by solid arrow in Fig. 5a. No matter compared with the center region in same cross section or the edge region of the back-end, the area proportion of the primary α-Al grains in edge region of the runner was obviously reduced. However, there were a fair amount of small size degenerated dendrites mixed in the near-spherical and spherical primary α-Al grains, as shown in Fig. 5b, so the grain diameter and shape factor reduced to 37 μm and 0.74 respectively. The secondary α_2-Al grains were mainly the equiaxed, granular and dendritic secondary α_2-Al grains except for some protrusions and the fine secondary α_2-Al dendrites, as shown in Fig. 5b.

3.3 Microstructure of the Mold Cavity

The Fig. 6a, c, e were the microstructures in center region of the near-end, middle-end and far-end of the mold cavity respectively, those positions were marked by "D","E" and "F" in Fig. 3, respectively. Their primary α-Al grains all were mainly included the spherical or near-spherical and rose-like ones, whose microstructure was essentially similar. However, the grain diameter and shape factor of the primary α-Al grains gradually reduced and improved respectively from near-end to far-end with the rheo-diecasting. The grain diameter of the primary α-Al grains in center regions of the near-end, middle-end and far-end were 37 μm, 36 μm and 35 μm, respectively, and the shape factor of the primary α-Al

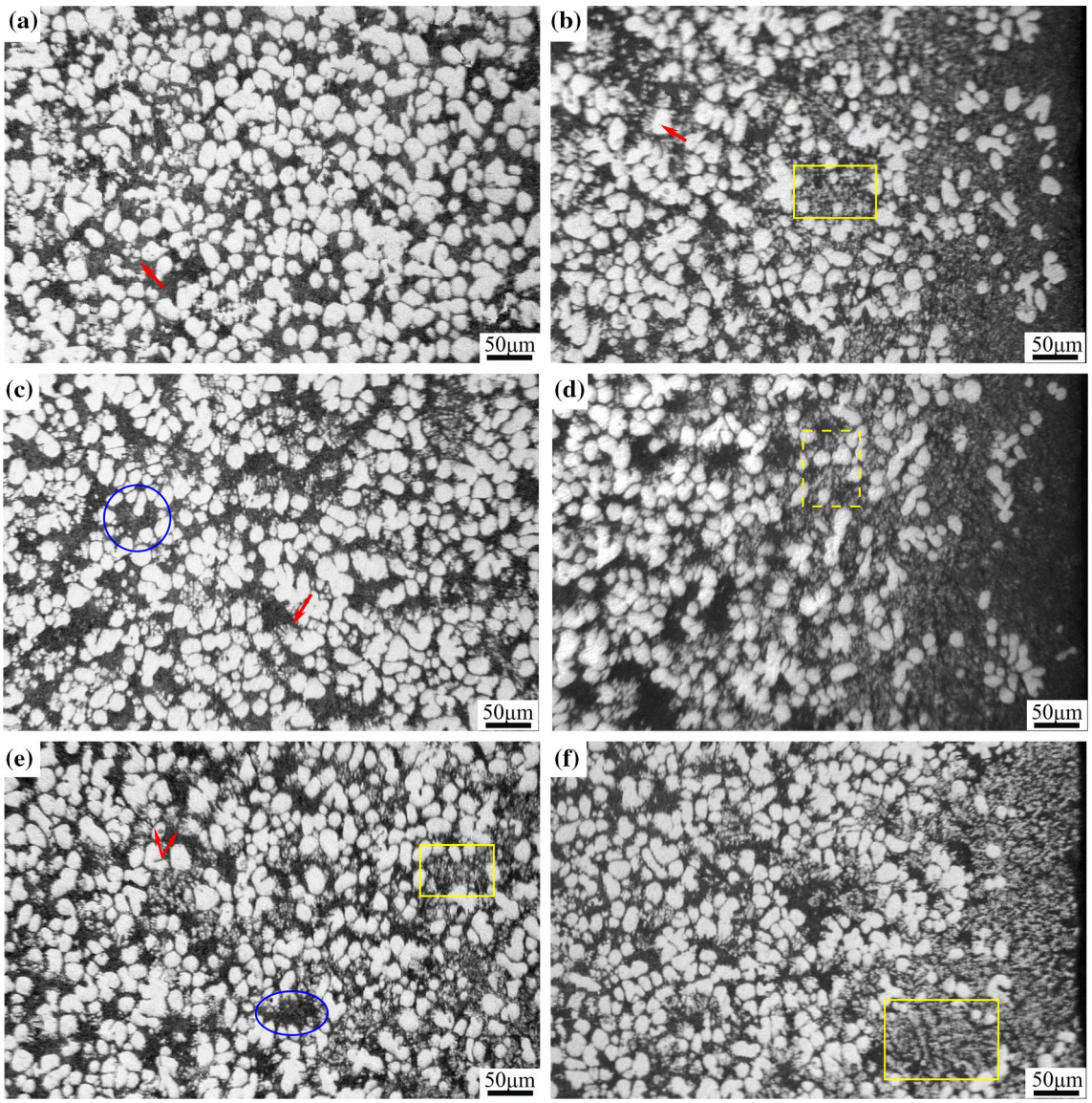

Fig. 6 Microstructures of the different positions of the mold cavity **a** center region of the near-end; **b** edge region of the near-end **c** center region of the middle-end; **d** edge region of the middle-end **e** center region of the far-end; **f** edge region of the far-end

grains in above regions were 0.77, 0.78 and 0.79, respectively. In addition, the area proportion of the primary α-Al grains gradually decreased from near-end to far-end, which promoted the gradually diverse morphologies of the secondary α_2-Al grains. There was few protrusions solidified into that by residual liquid in the near-end, and the secondary α_2-Al grains mainly were granular, as shown by arrow in Fig. 6a. In middle-end, the residual liquid solidified into protrusions on many primary α-Al grains, even some protrusions were dendrites, as shown by arrow in Fig. 6c, meanwhile, the residual liquid solidified into the pseudo-binary Al–Si eutectic structure in local regions, as shown by circle in Fig. 6c. Besides, there were many equiaxed, granular and rose-like secondary α_2-Al grains, as shown in Fig. 6c. In far-end, the residual liquid solidified into the protrusions and the pseudo-eutectic structure, as shown by arrows, ellipse in Fig. 6e, respectively. In addition, there were many granular and equiaxed secondary α_2-Al grains, moreover, the equiaxed secondary α_2-Al grains tended to merge into dendrites, as shown by rectangle in Fig. 6e.

Figure 6b, d, f showed the microstructures of the edge region of the near-end, middle-end and far-end, respectively. In near-end, there were some small size degenerated dendrites, rose-like and short rod-like primary α-Al grains, which made the grain diameter and shape factor decreased to 35 μm and 0.76, respectively, as shown in Fig. 6b. The residual liquid solidified into super fine equiaxed secondary α_2-Al grains in outmost edge region, meanwhile, it solidified into the protrusions near or away from the outmost edge region, as shown by arrow in Fig. 6b. It was worth noted that there were many dendrites, equiaxed and granular secondary α_2-Al grains those mixed together near the outmost edge region, as shown by rectangle in Fig. 6b. Compare with the near-end area proportion of the primary α-Al grains in middle-end edge region slightly decreased, moreover, the degenerated dendrites completely disappeared. The primary α-Al grains were mostly composed of near-spherical or spherical ones, whose grain diameter and shape factor were 34 μm and 0.77 respectively. The residual liquid solidified into the equiaxed secondary α_2-Al grains, protrusions and quenched microstructure, meanwhile, the equiaxed grains merged into the small size dendrites, as shown by rectangle in Fig. 6d. As shown in Fig. 6f, the area proportion of the primary α-Al grains in the far-end increased significantly comparing with the near-end and middle-end, moreover, the morphology of the secondary α_2-Al grains changed obviously they mostly were near-spherical and spherical, whose grain diameter and shape factor were 33 μm and 0.078 respectively. The secondary α_2-Al grains were consisted of equiaxed grains, protrusions and dendrites, even in some local regions the dendrites grew into the developed ones, as shown by rectangle in Fig. 6f.

4 Discussions

As shown in Fig. 7a, both of the grain diameter of primary α-Al grains in center region and edge region decreased along the rheo-diecasting direction, which might be affected by the rheo-diecasting system and the filling of the semi-solid slurry. On the one hand, the injection pressure made the bigger dendrites fracture when they passed through the narrow gate of the runner and ingate, as shown in Fig. 5a. On the other hand, the collision and friction among the primary α-Al grains made themselves break into the fragments during the filling of the semi-solid slurry, the difference among the Fig. 5a–c could support it. The refinement of the primary α-Al grains was mainly decided by the injection pressure, especially the fracture and bending of the dendrites, which could be expressed by formula (1) and (2). When the impact stress σ caused by injection pressure was higher than the yield strength

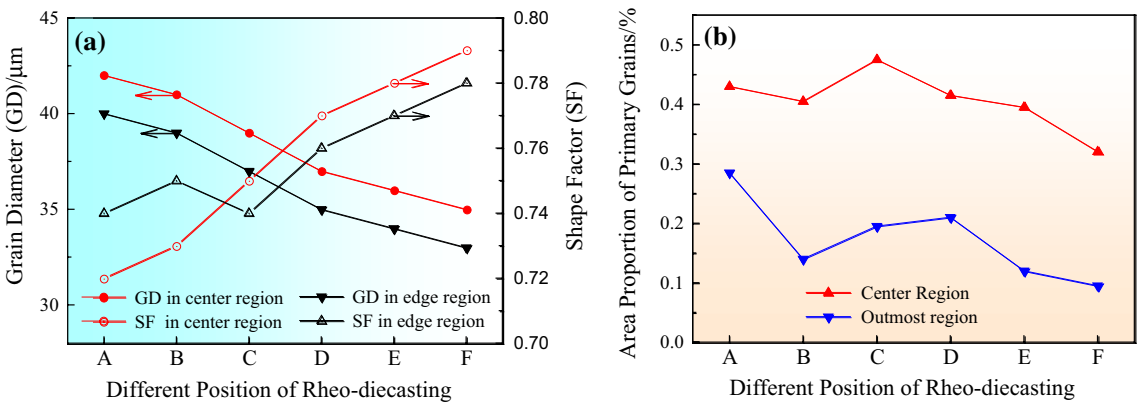

Fig. 7 Characteristic parameters and area proportion of the primary grains **a** characteristic parameters of the primary grains in different regions; **b** area proportion of the primary grains in different regions

at the necking of dendrite arm or the yield strength of the dendrites, the dendritic arms or the dendrites would be bent or even fractured [26].

$$\sigma = \frac{16\,P\,D\,l^3 \sin\alpha}{\pi d^3 wh} \tag{1}$$

$$\sigma = \frac{4P\,l^3 \sin\alpha}{\pi D^2 wh} \tag{2}$$

where σ is impact stress caused by injection pressure, P is injection pressure, D is diameter of the primary dendrite, l is the length of the dendritic arms, α is the angle between the direction of the injection pressure and dendritic arm, d the diameter at the necking of dendrite arm, w and h are the width and thickness of the mold cavity at the dendrite was fixed, respectively.

Closer observation would reveal that the decreasing of the grain diameter along rheo-diecasting direction was divided into the fast and slow decreasing stage. The grain diameter decreased quickly from front-end to near-end, but it decreased gently from the near-end to far-end, which might be related to the injection pressure loss. During the rheo-diecasting, the semi-solid slurry filled the mold cavity with laminar flow, moreover, it could be considered as non-Newtonian fluid which obeys the power law model. According to the Hargon–Poiseuille equation [27] and the Reynolds number equation of the laminar flow [28], the injection pressure loss of the semi-solid slurry in mold cavity with rectangle cross-section could be described by formulas (3) and (4) [20]. The injection pressure loss increased with filling time, and the refinement of the primary α-Al grains was weakened, which according to the formulas (1)–(4).

$$\Delta P = \int_0^t \frac{8K(w+h)}{f(w/h)}\left(\frac{v}{h}\right)^{n+1} dt \tag{3}$$

$$f(w/h) = 2\left[\frac{w}{h}+1\right]^2\left[\frac{1}{3} - \frac{64w}{\pi^5 h}\sum_{n=1}^{\infty}\tan\frac{\pi h^2(2n-1)}{w+h}/(2n-1)^5\right] \tag{4}$$

where t is the filling time, K is viscosity coefficient, v is the filling velocity, w and h are width and thickness of the mold cavity, respectively.

It was worth noted that the grain diameter in center region was bigger than that in edge region, which might be due to the chilling effect of the mold and the heat transfer between the semi-solid slurry and the mold. On the one hand, the residual liquid rapidly solidified as it contacted the mold, which greatly restricted the growth of the primary α-Al grains. On the other hand, the heat transfer between the center region and mold was relatively slow, moreover, the residual liquid solidification following the completion of the heat transfer occurred at a much slower rate, which is helpful for the Ostwald ripening of the primary α-Al grains [29]. A heat balance equation was used to evaluate the heat transfer between the semi-solid slurry and mold under the condition of the simplify assumptions, which was the formula (5) [30].

$$k(T - Tm)dSdt = -\rho CdVdT \tag{5}$$

$$C = C_0 - \frac{df_s(T)}{dT}L \tag{6}$$

where k is the heat transfer coefficient between semi-solid slurry and mold, T is the temperature of the semi-solid slurry unit, T_m is the temperature of the mold, S is the surface area of the heat transfer, ρ is the density of the semi-solid slurry, C is the specific heat of the semi-solid slurry, C_0 is the specific heat of the A380 melt, $df_s(T)/dT$ is the variation rate of the solid fraction with the temperature, L is the latent heat of solidification, and V is the volume of the semi-solid slurry unit. Thus, the formula (5) could be written as:

$$T_c = -\frac{dT}{dt} = \frac{2k(T - T_m)(w+h)}{wh\rho\left[C_0 - \frac{df_s(T)}{dT}L\right]} \tag{7}$$

where T_c is the cooling rate, w and h are width and thickness of the mold cavity, respectively.

Formula (7) clearly showed that the cooling rate of center region was lower comparing with the edge region as it had high temperature and longer distance of heat transfer. The empirical formula $D = BT_c^{-m}$ (D is grain diameter, B and m are the constants related to materials, T_c is cooling rate) illustrated the relationship between the cooling rate and grain size [30].

Above mentioned factors not only affected the primary grain diameter but also affected the shape factor, which made the shape factor of the center region improve gradually. However, the increasing of the shape factor included rapid and gentle increasing stage, coincidentally, the boundary of the two stages was the near-end that was same as that divided the change curves of the grain diameter into two stages, as shown in Fig. 7a. It could be inferred that when the dendrites bent or fractured, the sharp corners of the primary α-Al grains was broken or blunted. The spheroidization of the primary α-Al grains were improved as the filling process of the semi-solid slurry continued. The combination of injection pressure and narrow gate of the runner and ingate was the main reason for the rapid increase of shape factor from front-end to near-end. But the collision and friction among primary α-Al grains gradually became the main reasons for the increase of shape factor with the semi-solid slurry passed through ingate

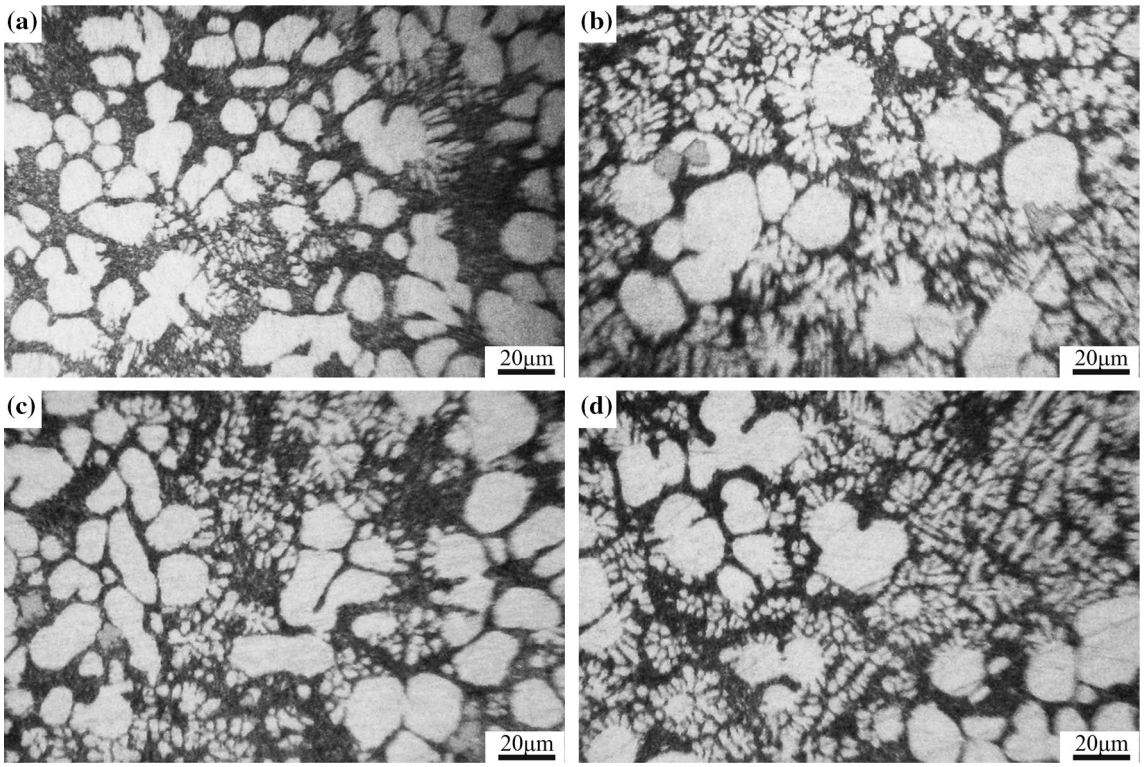

Fig. 8 Morphology of the secondary α_2-Al grains in rheo-diecastings **a** protrusions; **b** protrusion, fine dendrite and equiaxed grain; **c** granular and near-spherical grain; **d** dendrite and equiaxed grain

and the injection pressure decreased, therefore, the shape factor increasing slowly from near-end to far-end under the condition of the primary α-Al grains had got large refinement and spheroidization. There were two distinct stages in the change of shape factor in edge region those were quite different from that in center region. The shape factor in edge region was bigger than that in center regions from front-end to back-end, but the shape factor in edge region was smaller than that in center region from runner to far-end. At the first stage, the chilling effect of the shot sleeve and the rapid heat transfer of the edge region made the morphology of primary α-Al grain keep largely similar to that of the semi-solid slurry preparation stage. At the second stage, the primary α-Al grains were probably brought into edge region by the residual liquid from center region of the previous position, e.g., the primary α-Al grains in edge region of "E" *might come from the center region of "D". Therefore, the shape factor of the edge region was close to that of the previous center region, moreover, the change mechanism of the edge region in the second stage was similar to that of the center region, meanwhile, which also benefited from the chilling effect of the mold and the rapid heat transfer between semi-solid slurry and the mold.

In addition, the semi-solid slurry was easily divided into the leading and subsequent ones during whose filling because of the hysteresis of solid and the high freedom of the liquid. The former carried the less primary α-Al grains and mainly solidified in edge region, and the later solidified in center region. At the same cross section, the viscosity of the semi-solid slurry gradually increased to an approximate constants with the number of the primary α-Al grains increased, which made the area proportion of the primary α-Al grains gradually increased from edge region to center region and distributed evenly in center region, as shown from Figs. 4, 5 and 6. However, in rheo-diecasting direction, the viscosity of the semi-solid slurry increased with whose temperature decreased, which meant that the area proportion of the primary α-Al grains in center region and outmost edge region(extending 150 μm from the edge to inside) decreased with the filling, as shown in Fig. 7b. With the grain diameter decreased, the shape factor increased, and the area proportion of the primary α-Al grains decreased, the primary α-Al grains gradually distributed uniformly in center region from near-end to far-end. It was noteworthy that the area proportion of the primary α-Al grains in rheo-diecastings was bigger than that in the semi-solid slurry before entering shot

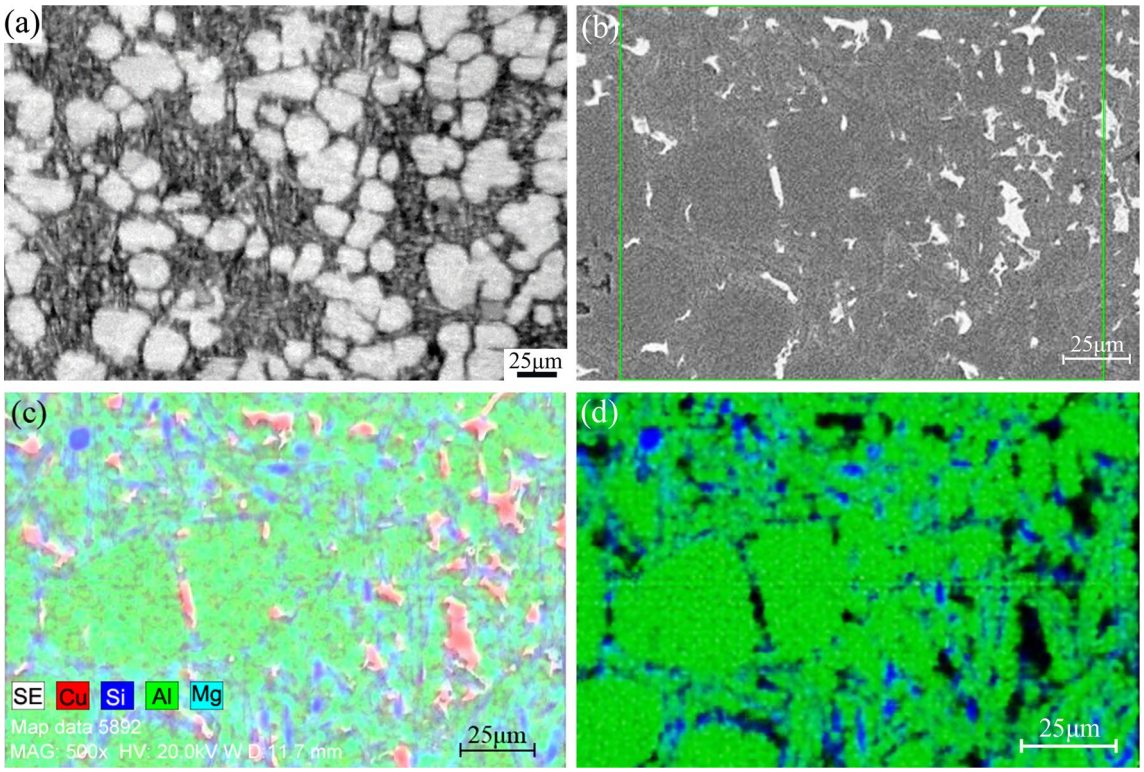

Fig. 9 Morphology of the pseudo Al–Si eutectic structure and main elements distribution **a** pseudo Al-Si eutectic structure; **b** SEM image; **c** distribution of main elements; **d** distribution of Al and Si elements

sleeve through comparing the Figs. 1 and 6a. Except for grain growth, it was mainly related to the nucleation of the residual liquid in shot sleeve [31], however, it was similar to that of the semi-solid slurry prepared by near liquidus casting [18]. Therefore, it was difficult to distinguish whether the primary α-Al grains formed in the early stage or in shot sleeve.

During rheo-diacasting, the accumulation of the primary α-Al grain fragments and secondary α_2-Al nuclei or grains formed in previous positions and the effective nucleation rate would make the morphology of the secondary solidification structure gradually present diversity. But the collision and fraction among the secondary α_2-Al grains and between the secondary α_2-Al grain and the primary α-Al grain, the chilling effect of the mold, and the heat transfer between the semi-solid slurry and the mold and the solute concentrations in the residual liquid could not be also ignored. The low sub-cooling and heat transfer made the residual liquid has the low effective nucleation rate in center region, resulting in the residual liquid firstly solidifying into the granular grains and the protrusions of the primary α-Al grains, as shown in Fig. 8a. However, the effective nucleation rate of the residual liquid was high in edge region under the condition of the chilling effect of the mold and the rapid heat transfer, which made the secondary α_2-Al grains mainly compose of the protrusions, equiaxed grains and fine dendrites, as shown in Fig. 8b. The secondary α_2-Al grains in edge region were difficult to break and bring into the semi-solid slurry while those in center region were easily broken into the small size rose-like secondary α_2-Al grains brought into the semi-solid to fill the mold as the nucleation sites. On the one hand, a part of the nucleation cores got further spheroidization and refinement during filling into center region. They became the nucleation cores of the granular or near-spherical secondary α_2-Al grains in center region under the low effective nucleation rate, but the residual liquid also took the primary α-Al grains as the nucleation sites to form protrusions in center region, as shown in Fig. 8c. It was worth noted that when the temperature of the semi-solid slurry decreased and the solute concentration of the residual liquid increased with the filling of the semi-solid slurry proceeded, the pseudo Al-Si eutectic structure might be formed in local center region under the condition of the slow heat transfer, as shown in Fig. 9. On the other hand, the other nucleation cores were brought into edge region. They grew into the developed secondary α_2-Al dendrites and rose-like secondary α_2-Al grains under the rapid heat transfer, meanwhile, the high effective nucleation rate of the residual liquid made a large number of the equiaxed secondary α_2-Al grains form, as shown in Fig. 8d. Therefore, the morphology of secondary

α_2-Al grains gradually presented more multiplex and complicate characteristics companied with the effective nucleus gradually accumulating and being brought into the semi-solid slurry.

5 Conclusions

1. The grain diameter and shape factor of primary α-Al grains decreased and increased along the rheo-diecasting direction, respectively, at the same time, the primary α-Al grains gradually distribute uniformly. However, the characteristic parameter changes of the primary α-Al grains were divided into fast and slow stages at the near-end of the mold cavity.
2. The combination of injection pressure and narrow gate of the runner and ingate made the characteristic parameters of the primary α-Al grains change quickly. With the semi-solid slurry passing the ingate and the primary α-Al grains getting large refinement and spheroidization, the collision and friction among primary α-Al grains became the main factors for the evolution of the primary α-Al grains, therefore, the morphology of the primary α-Al grains changed slowly.
3. The accumulation of the primary α-Al grain fragments, secondary α_2-Al nuclei or grains which formed in previous positions and the effective nucleation rate of the residual liquid that was controlled by the heat transfer between the semi-solid slurry and mold made the secondary solidification microstructure of the residual liquid present multiplex and complicate characteristics.

Acknowledgements National Basic Research Program of China (2011CB606300) supported this work.

References

1. M.C. Flemings, Behavior of metal alloys in the semisolid state. Metall. Trans. B **22**(3), 269–293 (1991)
2. D.K. Kirkwood, Semisolid metal processing. Int. Mater. Rev. **49**(5), 173–189 (1994)
3. O. Lashkari, R. Ghomashchi, The implication of rheology in semi-solid metal processes: An overview. J. Mater. Process. Technol. **182**(1–3), 229–240 (2007)
4. A. Blanco, Z. Azpilgain, J. Lozares, P. Kapranos, I. Hurtado, Rheological characterization of A201 aluminum alloy. Trans. Nonferrous Met. Soc. China **20**(9), 1638–1642 (2010)
5. X.P. Niu, B.H. Hu, I. Pinwill, H. Li, Vacuum assisted high pressure die casting of aluminium alloys. J. Mater. Process. Technol. **105**(1), 119–127 (2000)
6. H. Cao, M. Hao, C. Shen, P. Liang, The influence of different vacuum degree on the porosity and mechanical properties of aluminum die casting. Vac. **146**, 278–281 (2017)
7. T. Ito, T. Takikita, I. Miki, Wheels and Other Automotive Parts Through the Pore-Free Die Casting Process: SAE International Congress & Exposition, Detroit, Michigan, U.S.A., 1991,SAE Technical Paper Series-910552 (1991) pp. 1–12
8. G. Bar-Meir, Analysis of mass transfer process in the pore free technique. J. Eng. Mater. Technol. **117**(2), 215–219 (1995)
9. B.K. Kang, C.P. Hong, Y.S. Jang, B.H. Choi, L. Sohn, Effect of casting parameters on the microstructure and mechanical properties of ADC10 alloys using a semisolid die casting and heat treating process. Mater. Trans. **57**(3), 410–416 (2016)
10. Z.Y. Liu, W.M. Mao, W.P. Wang, Z.K. Zheng, Investigation of rheo-diecasting mold filling of semi-solid A380 aluminum alloy slurry. Int. J. Min. Met. Mater. **24**(6), 691–700 (2017)
11. J. Ren, J. Ouyang, T. Jiang, An improved particle method for simulation of the non-isothermal viscoelastic fluid mold filling process. Int. J. Heat Mass Transf. **85**, 543–560 (2015)
12. R. Canyook, R. Utakrut, C. Wongnichakorn, K. Fakpan, S. Kongiang, The effects of heat treatment on microstructure and mechanical properties of rheocasting ADC12 aluminum alloy. Mater. Today: Proc. **5**(3), 9476–9482 (2018)
13. Y. Wang, S. Zhao, C. Zhang, Microstructures and mechanical properties of semi-solid squeeze casting ZL104 connecting rod. Trans. Nonferrous Met. Soc. China **28**(2), 235–243 (2018)
14. Q. Han, S. Viswanathan, The use of thermodynamic simulation for the selection of hypoeutectic aluminum-silicon alloys for semi-solid metal processing. Mater. Sci. Eng. A **364**(1–2), 48–54 (2004)
15. Z. Ma, H. Zhang, W. Song, X. Wu, J. Lina, H. Zhang, Pressure-driven mold filling model of aluminum alloy melt semi-solid slurry based on rheological behavior. J. Mater. Sci. Technol. **39**(15), 14–21 (2020)
16. C.G. Kang, J.S. Choi, Effect of gate shape and forging temperature on the mechanical properties in the injection forging process of semi-solid aluminum material. J. Mater. Process. Technol. **73**(1–3), 251–263 (1998)
17. P.K. Seo, D.U. Kim, C.G. Kang, The effect of the gate shape on the microstructural characteristic of the grain size of Al–Si alloy in the semi-solid die casting process. Mater. Sci. Eng. A **445–446**, 20–30 (2007)
18. P. Sharifi, J. Jamali, K. Sadayappan, J.T. Wood, Grain size distribution and interfacial heat transfer coefficient during solidification of magnesium alloys using high pressure die casting process. J. Mater. Sci. Technol. **34**(2), 324–334 (2018)
19. S. Otarawanna, N. Denmud, B. Vetayanugul, C. Phongphisutthinan, Microstructure characteristics of the surface layer in high-pressure die castings. Int. J. Cast Met. Res. **28**(6), 356–364 (2015)
20. M. Hitchcock, Y. Wang, Z. Fan, Secondary solidification behaviour of the Al–Si–Mg alloy prepared by the rheo-diecasting process. Acta Mater. **55**(5), 1589–1598 (2007)
21. Z. Fan, G. Liu, Solidification behaviour of AZ91D alloy under intensive forced convection in the RDC process. Acta Mater. **53**(16), 4345–4357 (2005)
22. M. Li, Y.D. Li, G.L. Bi, X.F. Huang, T.J. Chen, Y. Ma, Solidification behavior of 6061 wrought aluminum alloy during rheo-diecasting process with self-inoculation method. Trans. Nonferrous Met. Soc. China **28**(5), 879–889 (2018)
23. M. Li, Y.D. Li, G.L. Bi, X.F. Huang, T.J. Chen, Y. Ma, Solidification behavior and rheo-diecasting microstructure of A356 aluminum alloy prepared by self-inoculation method. China Foundry **14**(1), 1–9 (2017)
24. Z.Y. Liu, W.M. Mao, W.P. Wang, Z.K. Zheng, Preparation of semi-solid A380 aluminum alloy slurry by serpentine channel. Trans. Nonferrous Met. Soc. China **25**(5), 1419–1426 (2015)

25. C.M. Gourlay, A.K. Dahle, T. Nagira, N. Nakatsuka, K. Nogita, K. Uesugi, Granular deformation mechanisms in semi-solid alloys. Acta Mater. **59**(12), 4933–4943 (2011)
26. J.G. Barry, M.G. James, Mechanics of Materials 9th., CENGAGE Learning, Boston, U.S.A., (2018) pp. 390–488
27. J.H. Spurk, N. Aksel, *Fluid Mechanics*, 2nd edn. (Springer, Leipzig, 2008), pp. 175–184
28. R.B. Bird, R.C. Armstrong, O. Hassager, *Dynamics of Polymeric Liquids Volume 1 Fluid Mechanics* (Wiley, New York, 1987), pp. 295–339
29. L. Ratke, P.W. Voorhees, *Growth and Coarsening-Ostwald Ripening in Material Processing* (Springer, New York, 2002), pp. 117–126
30. T. Egami, W.L. Johnson, *Elements of Rapid Solidification-Fundamentals and Applications*, vol. 29 (Springer, Berlin, 1998), pp. 24–42
31. P. Wang, G.M. Lu, J.Z. Cui, Microstructure of nearby liquidus semi-continuous casting aluminum alloy A356. Acta Metall. Sin. **38**(4), 389–392 (2002)

Publisher's Note Springer Nature remains neutral with regard to jurisdictional claims in published maps and institutional affiliations.